Supporting Information

for

Designing a multifunctional AIE active fluorescent Schiff base probe: Sensitive heavy metal ions recognition and water induced aggregation

Heena,[a] Sudhanshu Naithani,[a] Sangeeta,[b] Biswajit Guchhait,[b] Tapas Goswami,[a*] Sushil Kumar[a*]

[a]*Department of Chemistry, Applied Science Cluster, University of Petroleum and Energy Studies (UPES), Dehradun-248007, Uttarakhand, India.*

[b]*Department of Chemistry, School of Natural Sciences, Shiv Nadar Institution of Eminence, Delhi-NCR, Uttar Pradesh 201314, India.*

Email: sushilvashisth@gmail.com; tgoswami@ddn.upes.ac.in

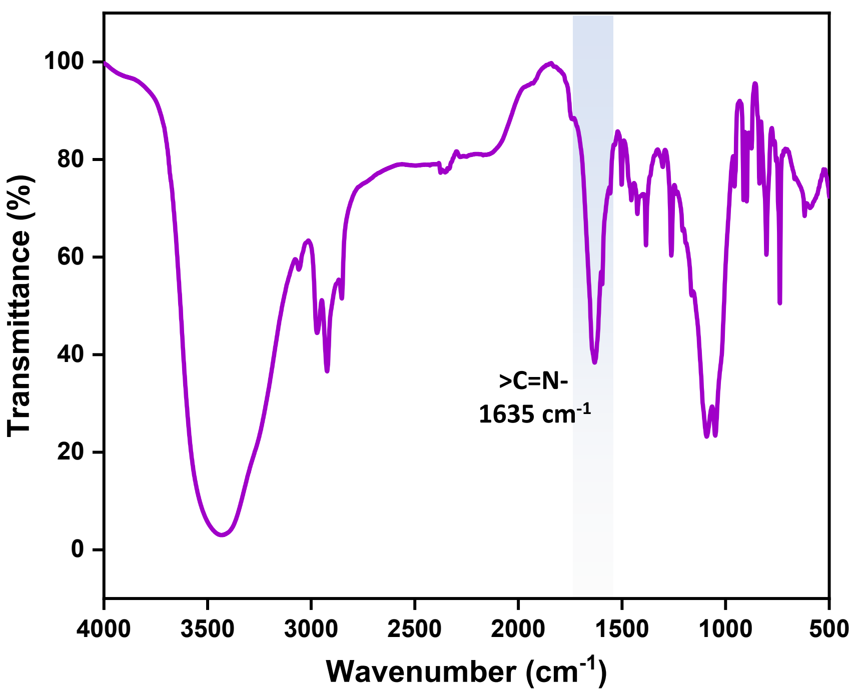

Fig. S1. FT-IR spectrum of **AnQn**.

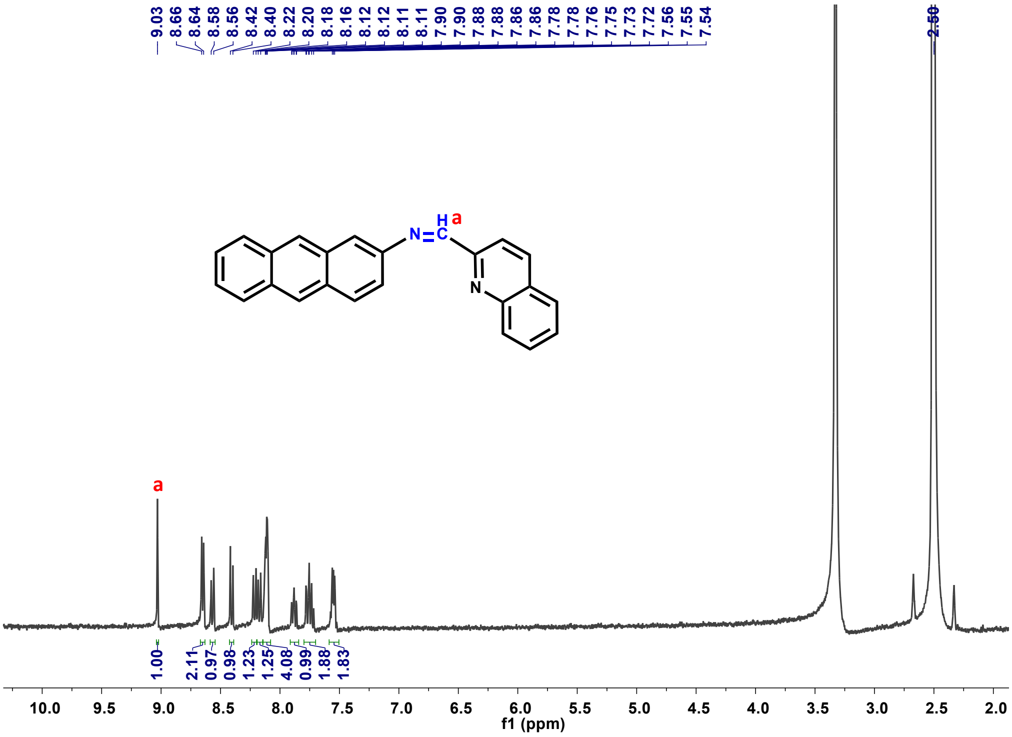

Fig. S2. ^{1}H NMR spectrum of **AnQn** in DMSO-d^6 at room temperature.

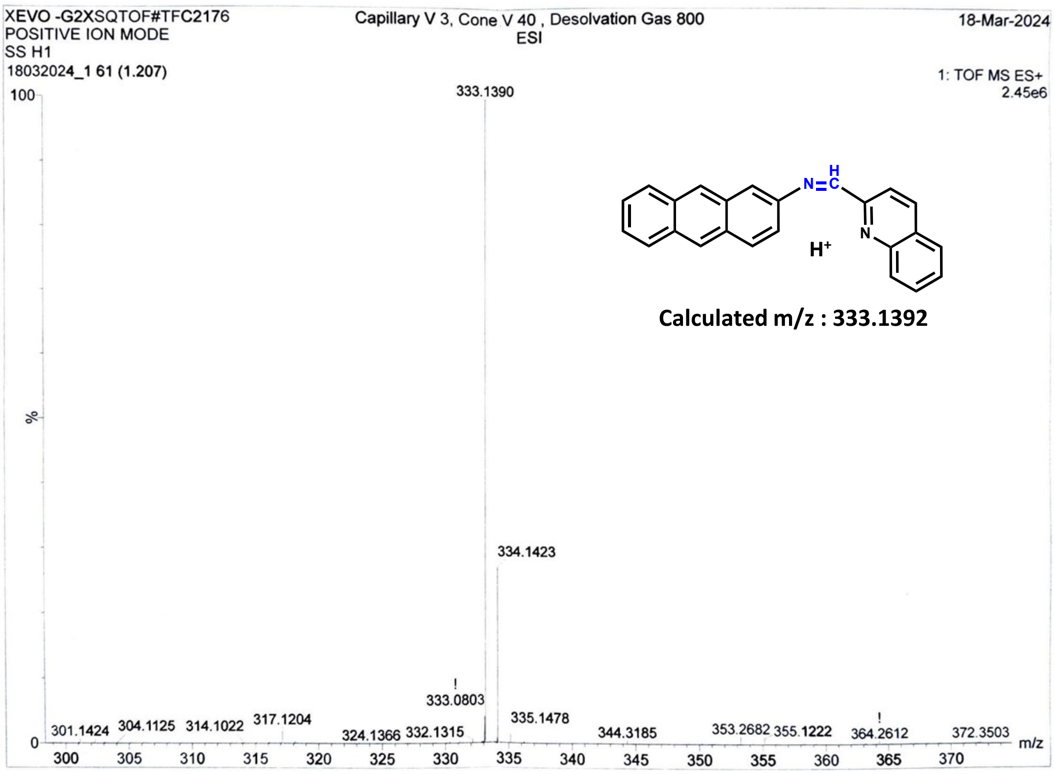

Fig. S3. ESI-MS of **AnQn** in CH_3CN solution at room temperature.

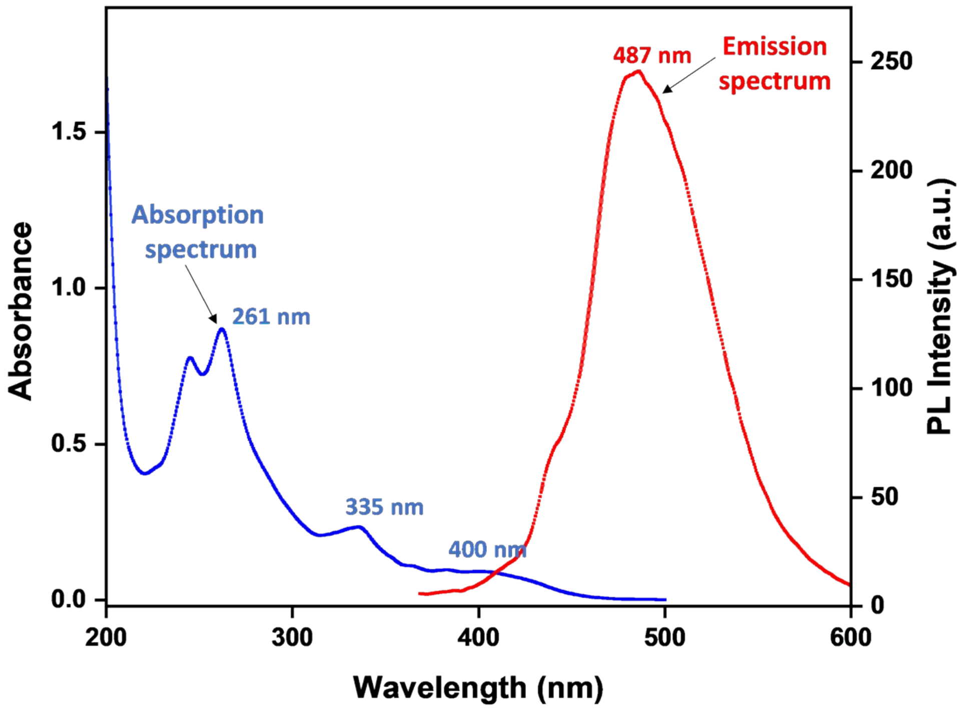

Fig. S4. Absorption and emission spectra of **AnQn** in CH_3CN solution.

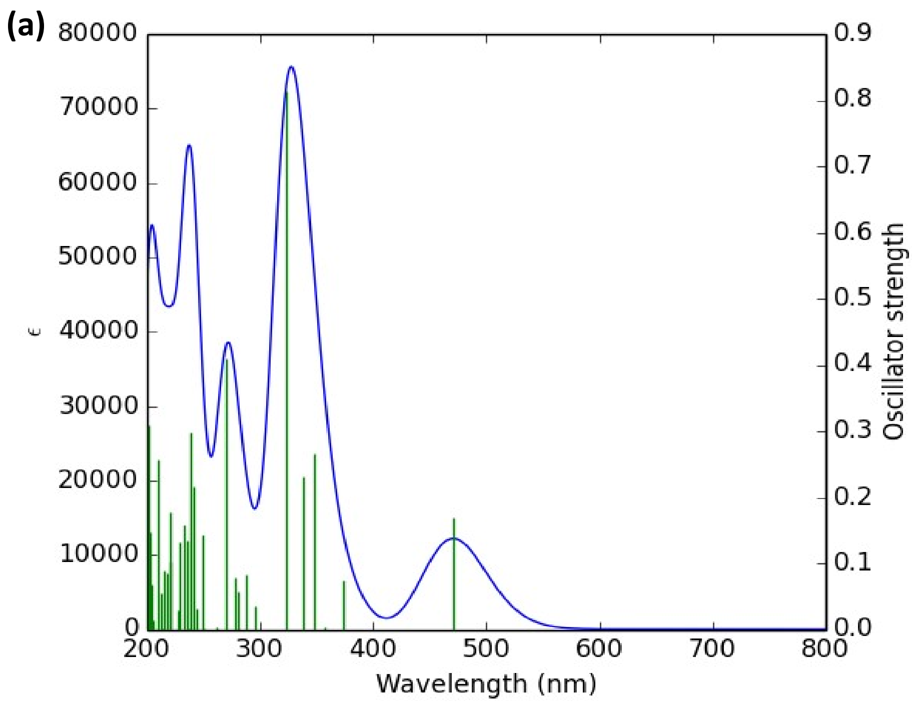

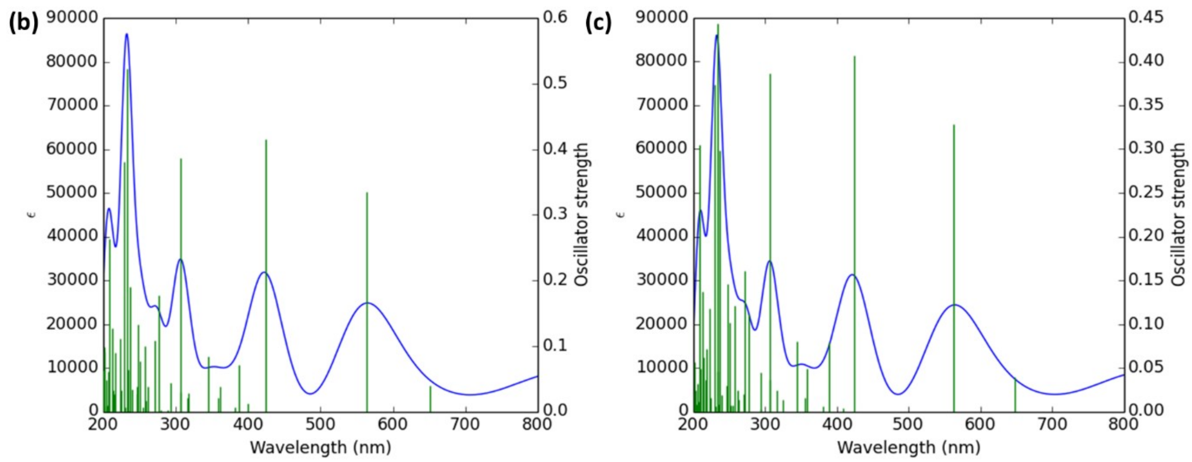

Fig. S5. Theoretically determined absorption spectra of (a) **AnQn** (b) **AnQn** -Al^{3+} and (c) **AnQn** -Ga^{3+}.

Table S1. Comparison of experimentally determined and theoretically calculated absorption bands

AnQn		AnQn-Al^{3+}		AnQn-Ga^{3+}		
Exp. λ_{max} (nm)	**Theo. λ_{max} (nm)**	**Exp. λ_{max} (nm)**	**Theo. λ_{max} (nm)**	**Exp. λ_{max} (nm)**	**Theo. λ_{max} (nm)**	**Transitions**
245	238	252	233	252	233	Quin $_{\pi-\pi^*}$
261	272		272		268	Quin $_{n-\pi^*}$
335	328	339	307	336	307	Anth $_{\pi-\pi^*}$
360-410	471	355-400	421	355-376	421	ICT
		485	564	490	562	LMCT

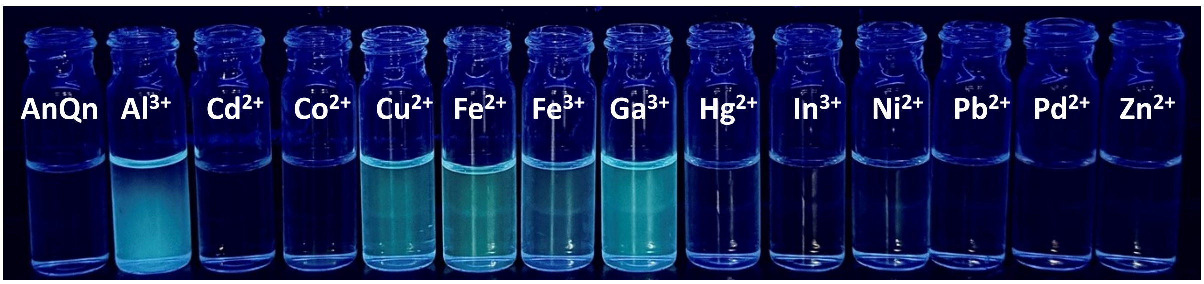

Fig. S6. Photographs of CH_3CN solutions of **AnQn** in presence of different metal ions under UV light illumination.

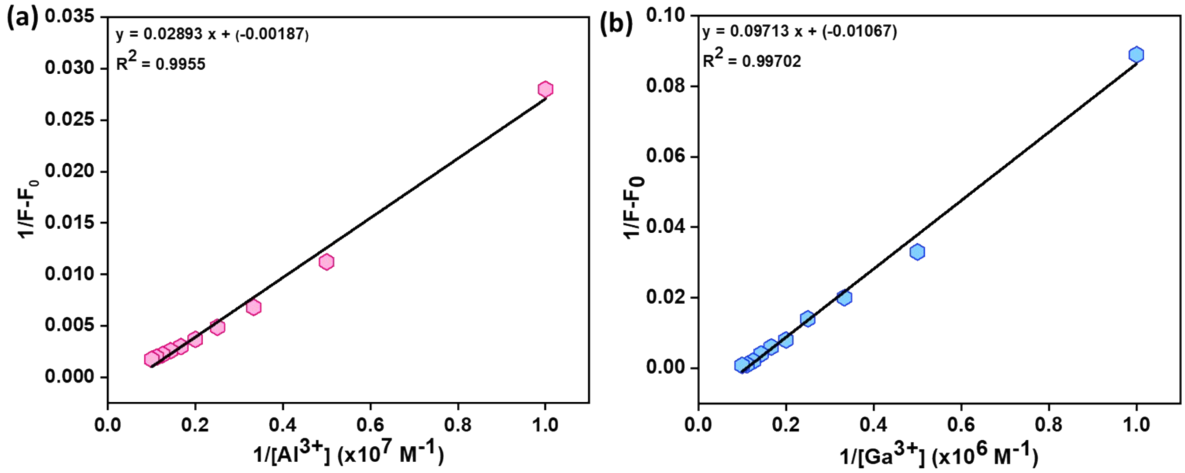

Fig. S7. Benesi-Hildebrand plots for determination of binding constant values for (a) **AnQn**-Al^{3+} and (b) **AnQn**- Ga^{3+} adducts.

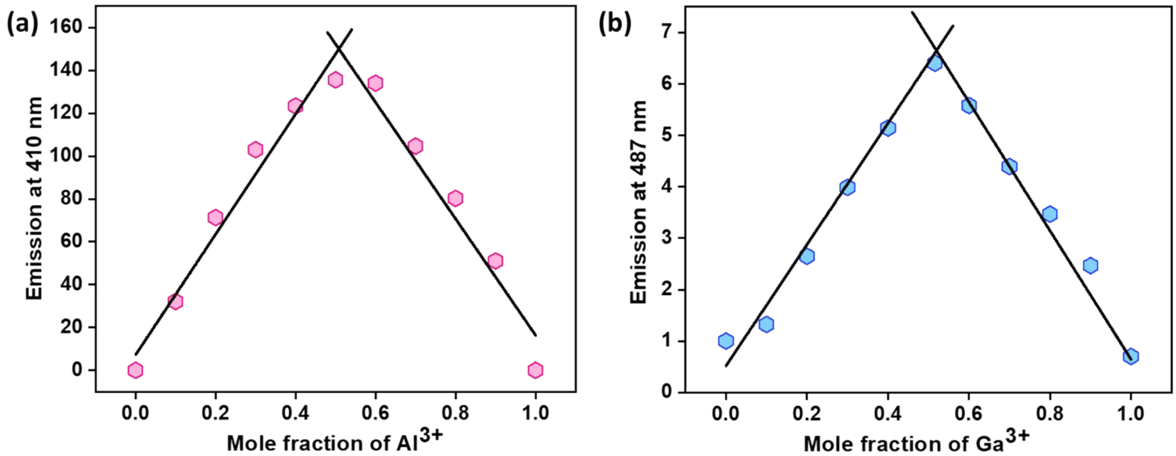

Fig. S8. Job's plot analysis for (a) **AnQn**-Al^{3+} and (b) **AnQn**-Ga^{3+}.

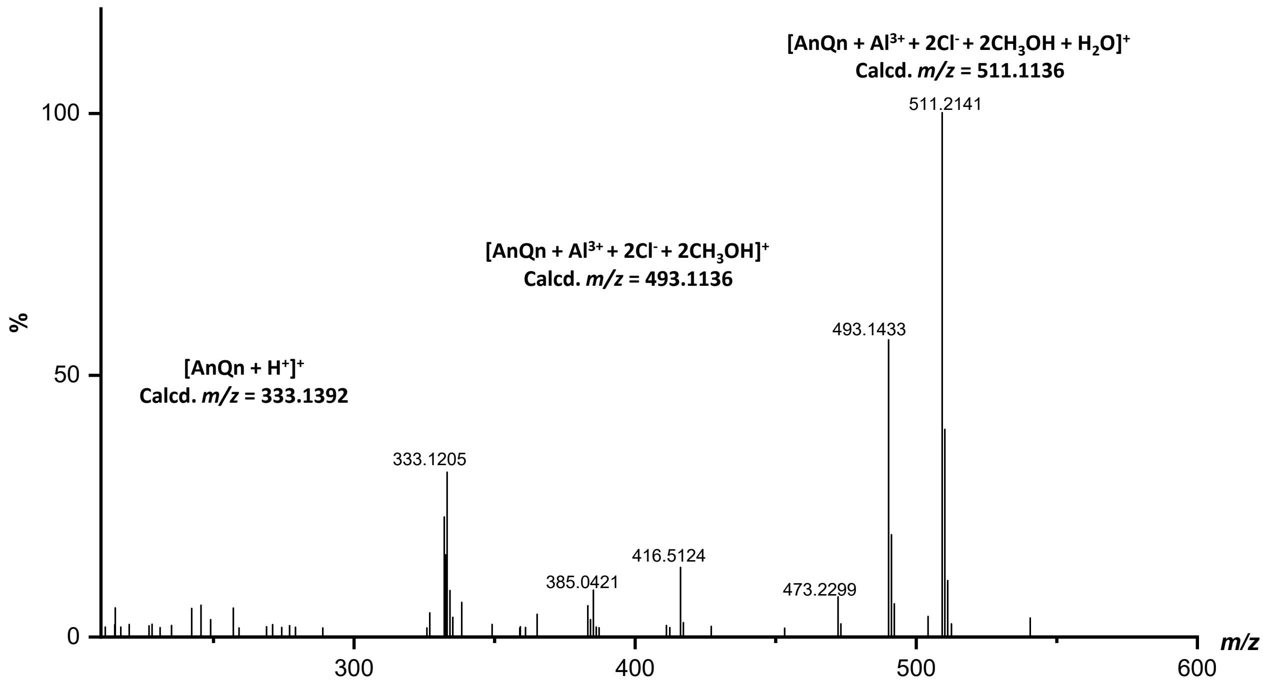

Fig. S9. ESI-MS of **AnQn**-Al^{3+} in CH_3OH solution.

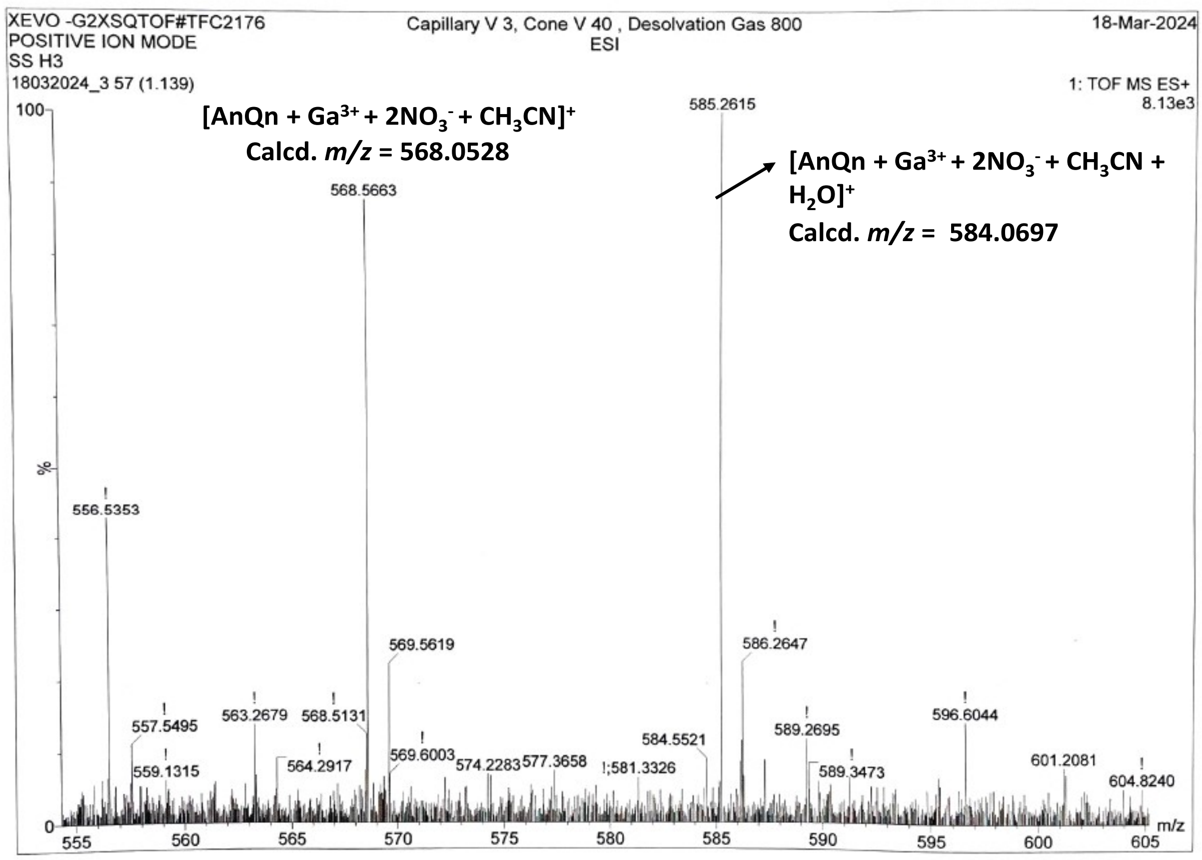

Fig. S10. ESI-MS of **AnQn**-Ga^{3+} in CH_3CN solution.

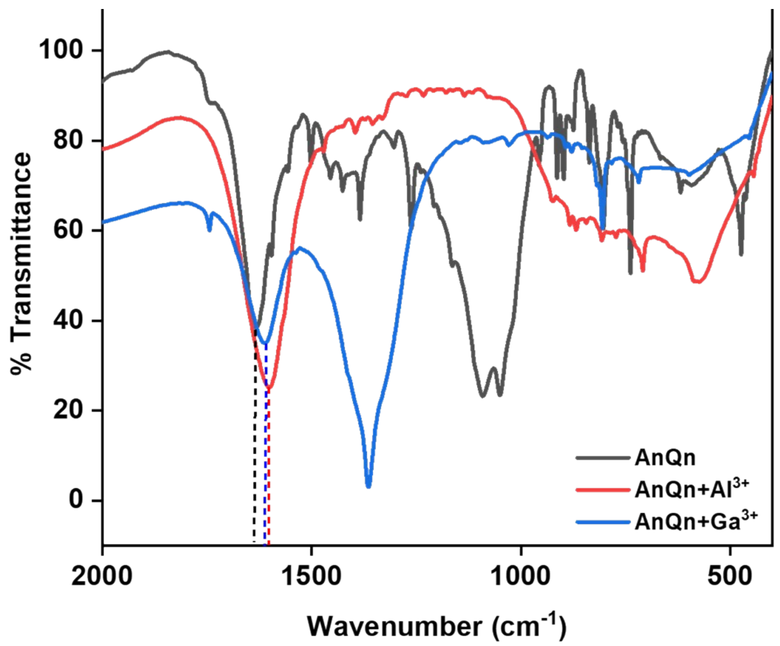

Fig. S11. FT-IR spectra of **AnQn** in presence of Al^{3+} and Ga^{3+} ions.

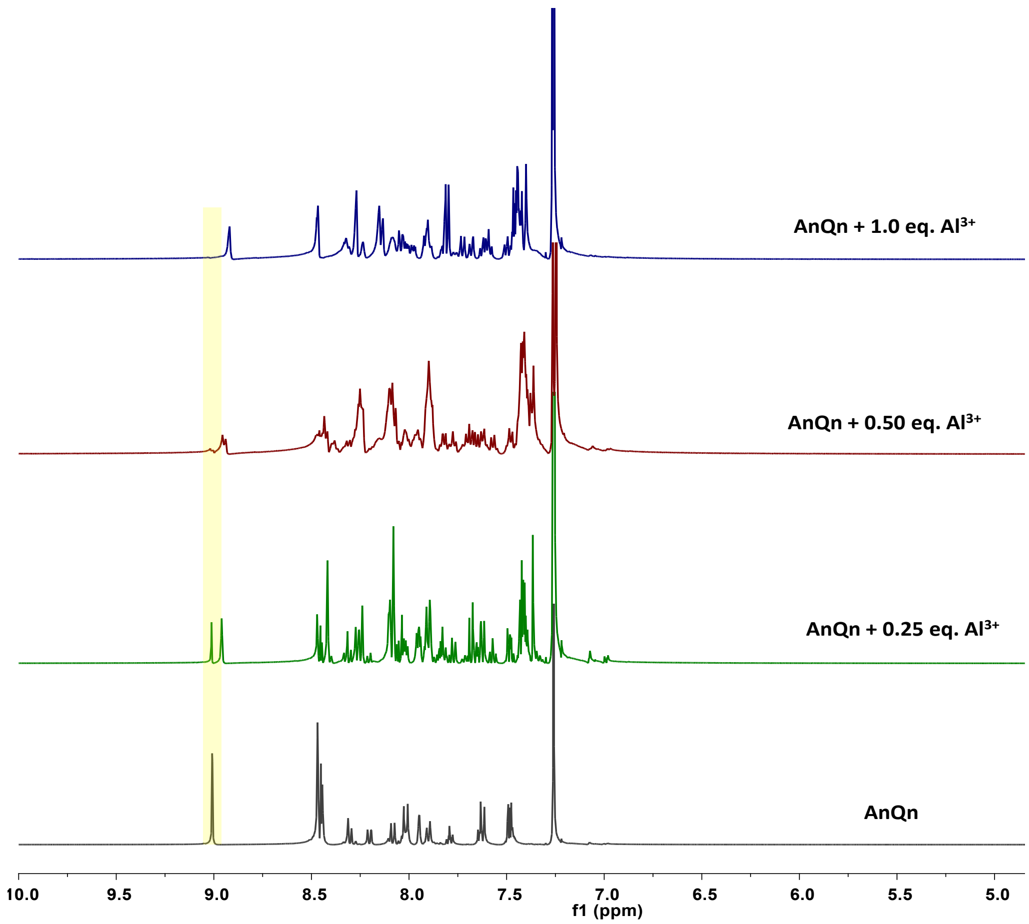

Fig. S12. ^{1}H NMR titration of **AnQn** in presence of Al^{3+} (0-1.0 eq.).

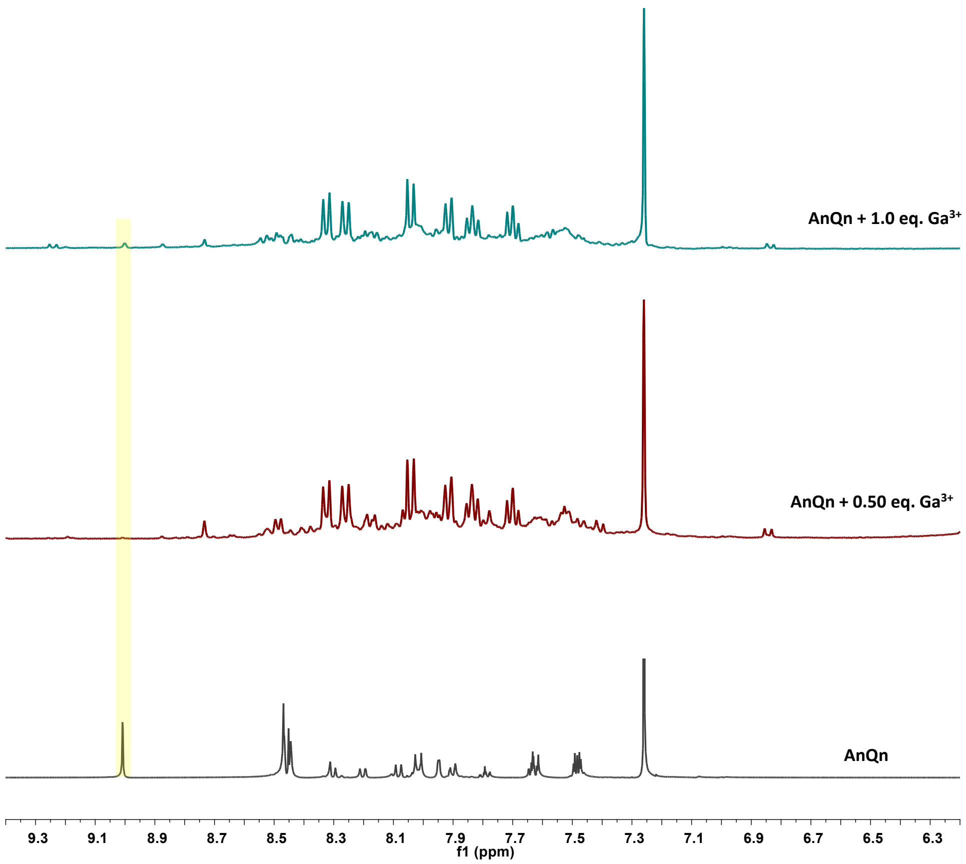

Fig. S13. ^{1}H NMR titration of **AnQn** in presence of Ga^{3+} (0-1.0 eq.).

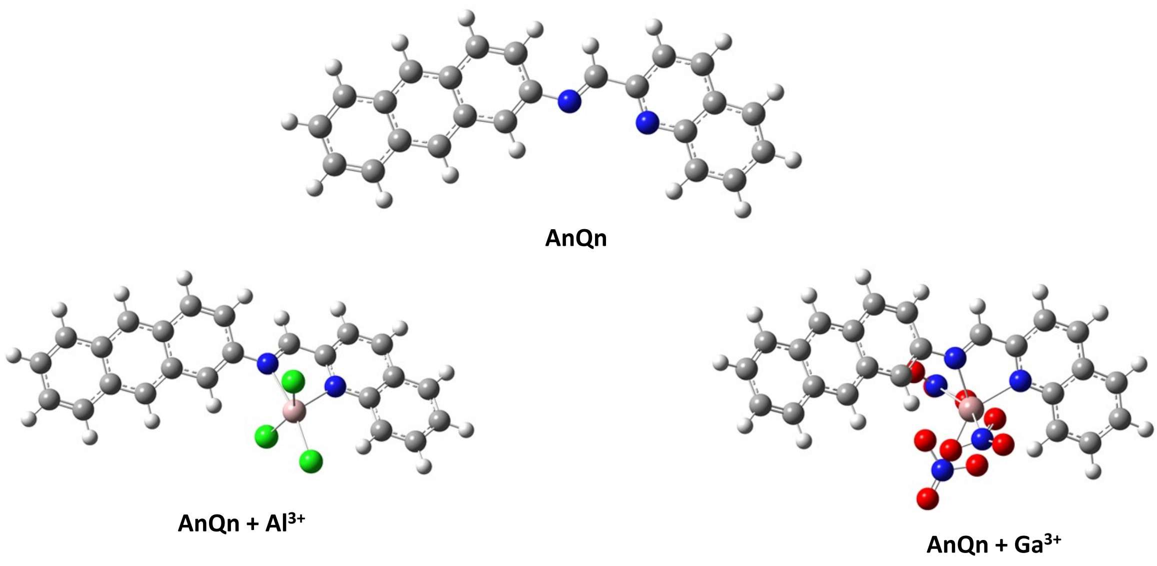

Fig. S14. Energy optimized structures of **AnQn** and its complexes **AnQn**-Al^{3+} and **AnQn**-Ga^{3+}. Color code: C (dark gray), N (blue), H (white), O (Red), Al (light pink), Cl (green) and Ga (light pink).

Table S2. Theoretically calculated selected bond parameters in complexes **AnQn**-Al^{3+} and **AnQn**-Ga^{3+}.

AnQn-Al^{3+}		**AnQn**-Ga^{3+}	
N_{imine} -Al- N_{quino}	79.42016°	N_{imine} -Ga- N_{quino}	81.16566
N_{imine} -Al	2.18038 Å	N_{imine} -Ga	2.083438 Å
N_{quino} -Al	2.08508 Å	N_{quino} -Ga	2.10987 Å

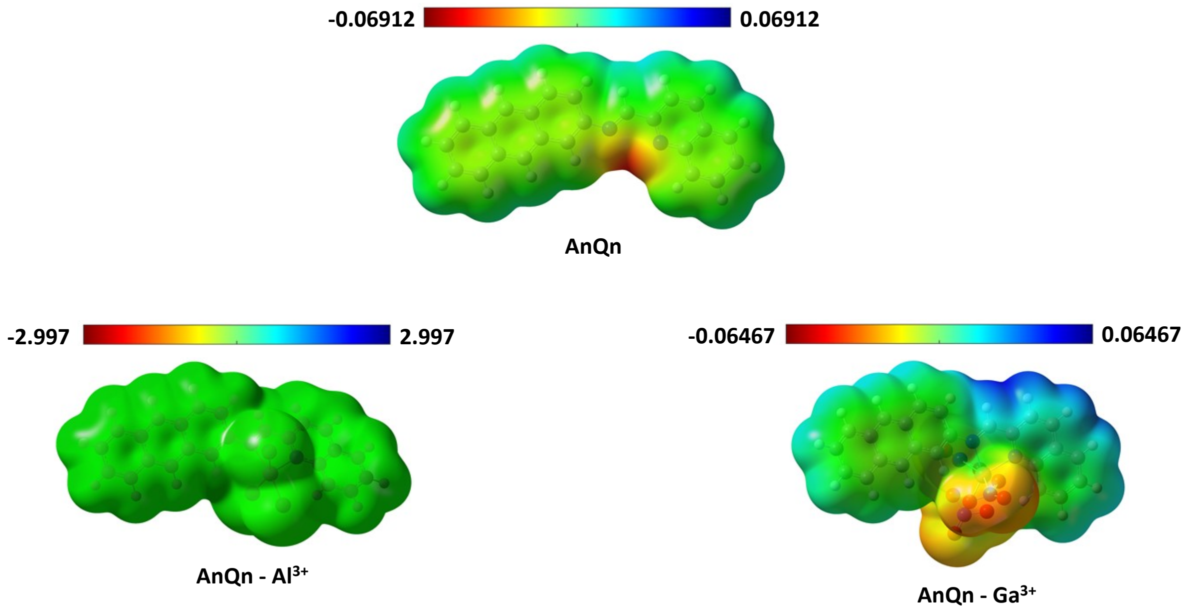

Fig. S15. Electrostatic potential maps (ESPs) of **AnQn**, **AnQn**-Al^{3+} and **AnQn**-Ga^{3+} calculated using the B3LYP/6-311G(d,p) basis set.

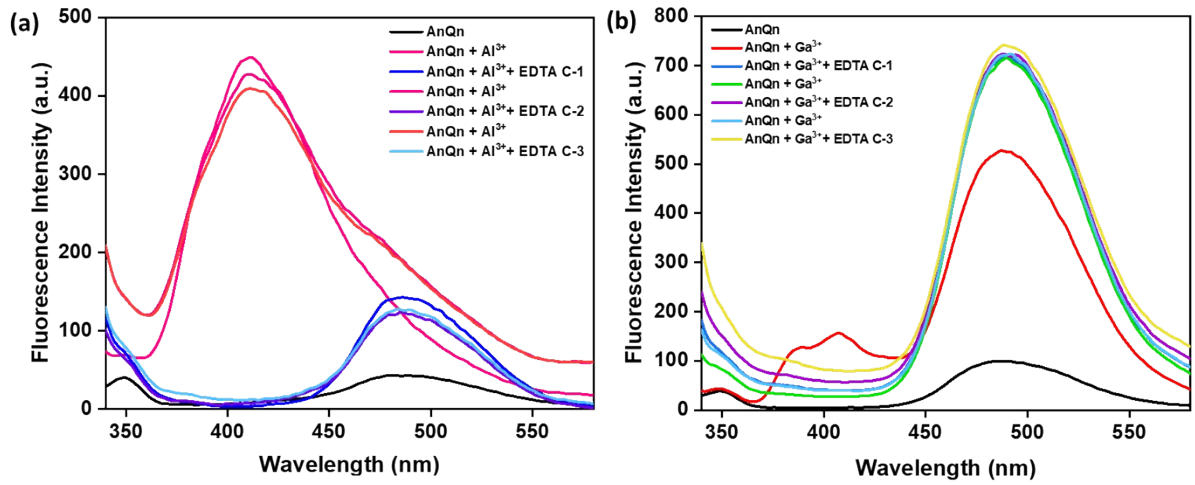

Fig. S16. Reversibility cycle of **AnQn** with (a) Al^{3+} and EDTA, and (b) Ga^{3+} and EDTA.

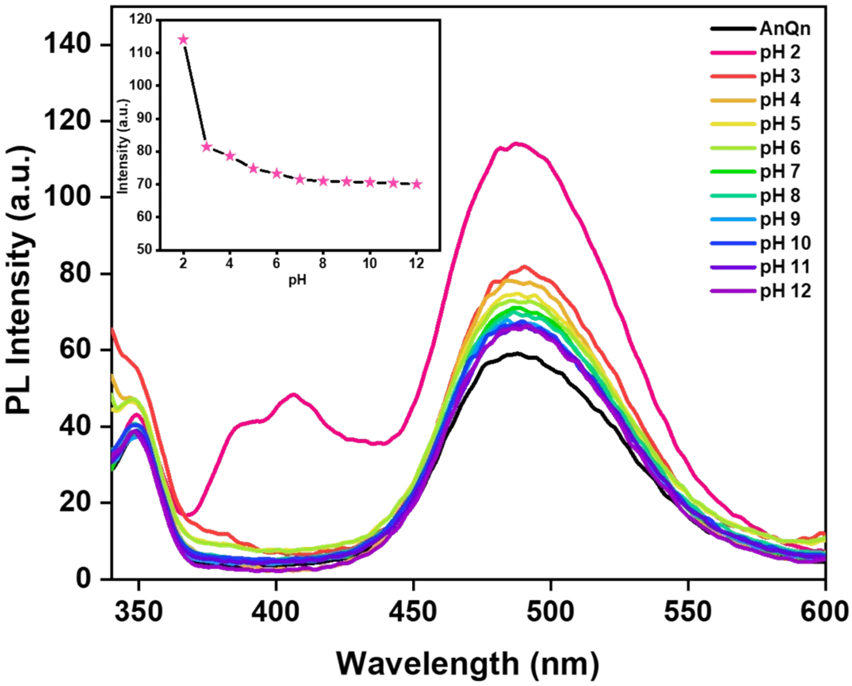

Fig. S17. Effect of pH on the fluorescence intensity of **AnQn**.

Table S3. Detection of Al^{3+} in real samples.

Real Sample	**Al^{3+} added (μM)**	**Al^{3+} detected (μM)**	**% Recovery**
Tap water	3.33	3.26	97.8
	6.67	6.8	101.9
	10	10.05	100.5
Soil water	3.33	3.18	95.4
	6.67	6.42	96.2
	10	10.02	100.2

Table S4. Detection of Ga^{3+} in real samples.

Real Sample	Ga^{3+} added (µM)	Ga^{3+} detected (µM)	% Recovery
Tap water	5	4.87	97.4
	10	10.06	100.6
	15	14.64	97.6
Soil water	5	4.98	99.6
	10	9.91	99.1
	15	15.03	100.2

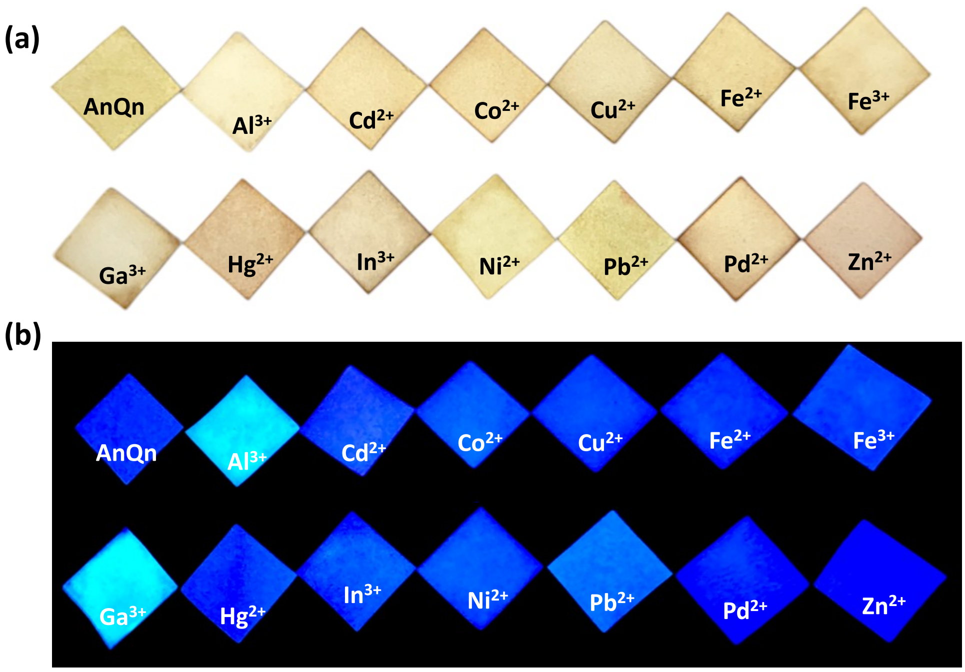

Fig. S18. Test strips of **AnQn** treated with different metal ions under (a) visible light and (b) UV light illuminations.

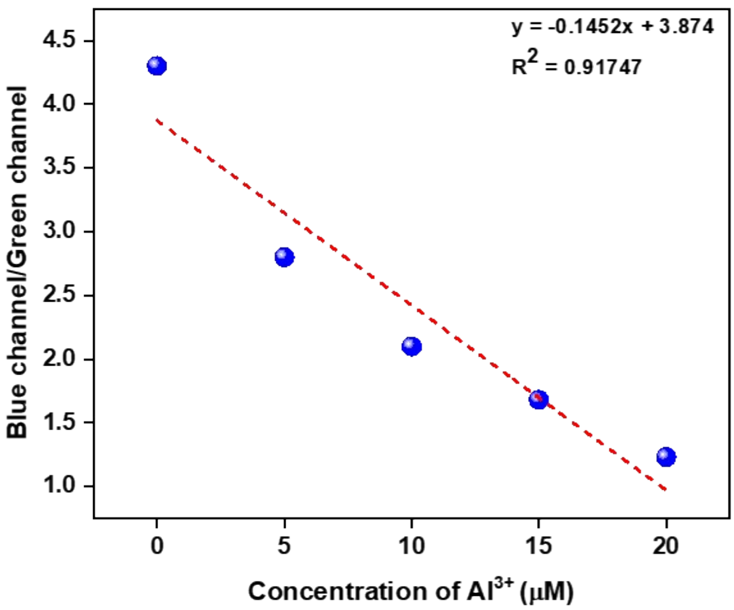

Fig. S19. Plot of RGB values (Blue/Green channel) and concentration of Al^{3+} for determination of detection limit using paper strips.

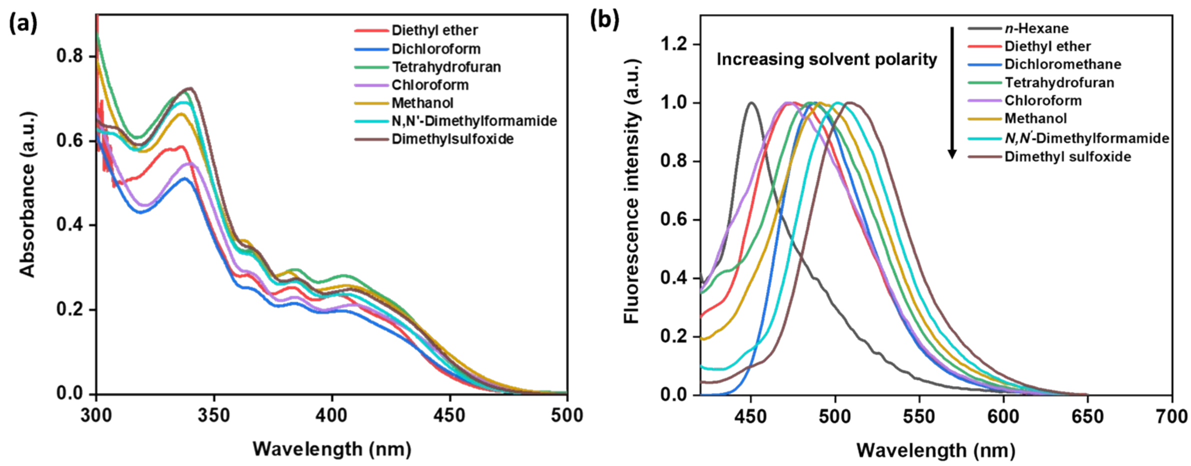

Fig. S20. Effect of different solvents on (a) absorption and (b) emission features of **AnQn**.

Table S5. Effect of solvent's polarity on optical characteristics of **AnQn**.

Solvent	**$\lambda_{absorption}$ (nm)**	**$\lambda_{emission}$ (nm)**	**$\lambda_{absorption}$ - $\lambda_{emission}$ (nm)**	**Stoke Shift (cm^{-1})**
Diethyl ether	332	473	141	70921.99
Dichloromethane	338	487	149	67114.09
Tetrahydrofuran	336	486	150	66666.67
Chloroform	340	470	130	76923.08
Methanol	336	492	156	64102.56
N,N'-Dimethylformamide	339	501	162	61728.40
Dimethylsulfoxide	340	508	168	59523.81

Table S6. Time-resolved fluorescence parameters of **AnQn** with increasing water fractions.

Sample	**τ_1 (ns)**	**τ_2 (ns)**	**τ_{av} (ns)**	**χ^2**
AnQn (in ACN)	1.82	9.79	6.89	1.06
AnQn (30% water)	19.39	-	19.39	1.039
AnQn (40% water)	21.17	-	21.17	1.025
AnQn (50% water)	23.32	-	23.32	1.062
AnQn (60% water)	25.17	-	25.17	1.018
AnQn (70% water)	23.93	-	23.93	1.025

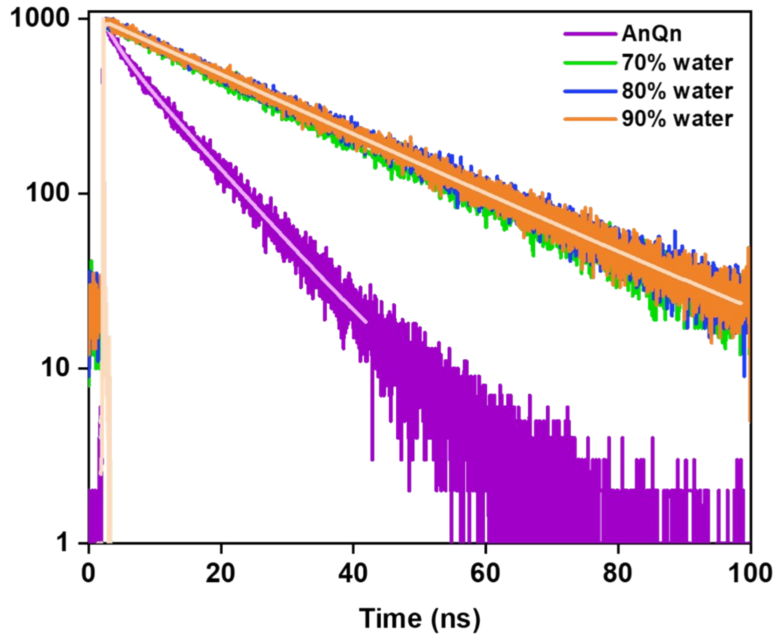

Fig. S21. TRF data of **AnQn** in acetonitrile with varied water fractions from 70%-90%.

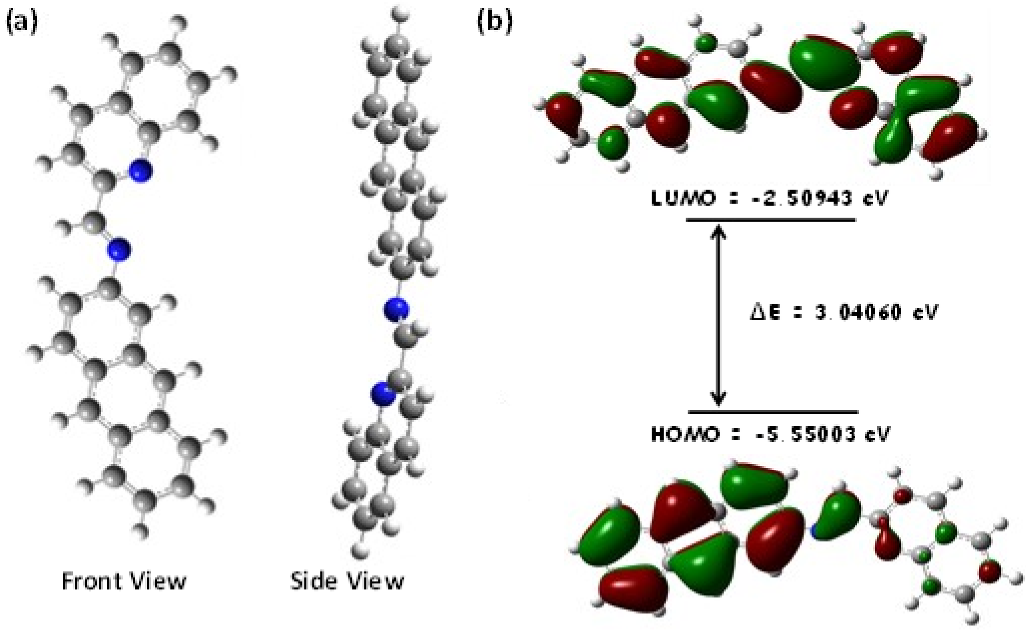

Fig. S22. (a) Energy optimized structures of **AnQn** and (b) HOMO-LUMO energy levels of **AnQn**.

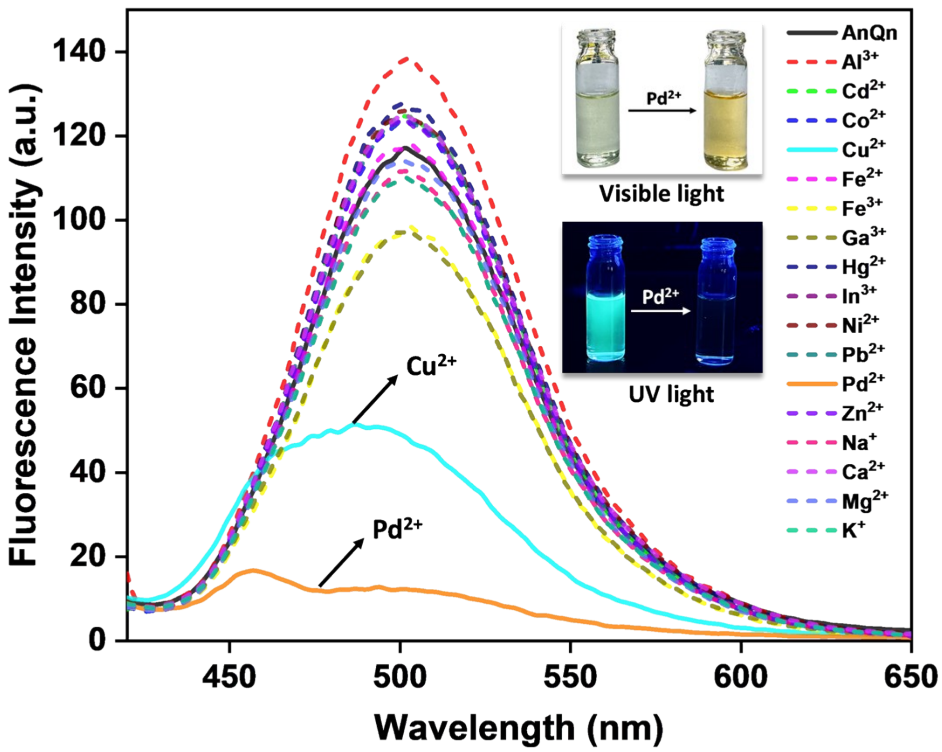

Fig. S23. Change in emission spectral intensity of **AnQn** (1.0 μM) in presence of various metal ions (3.0 μM) in (CH_3CN: H_2O, 4:6, v/v). Inset: Visual color changes observed upon addition of Pd^{2+} under UV as well as visible light.

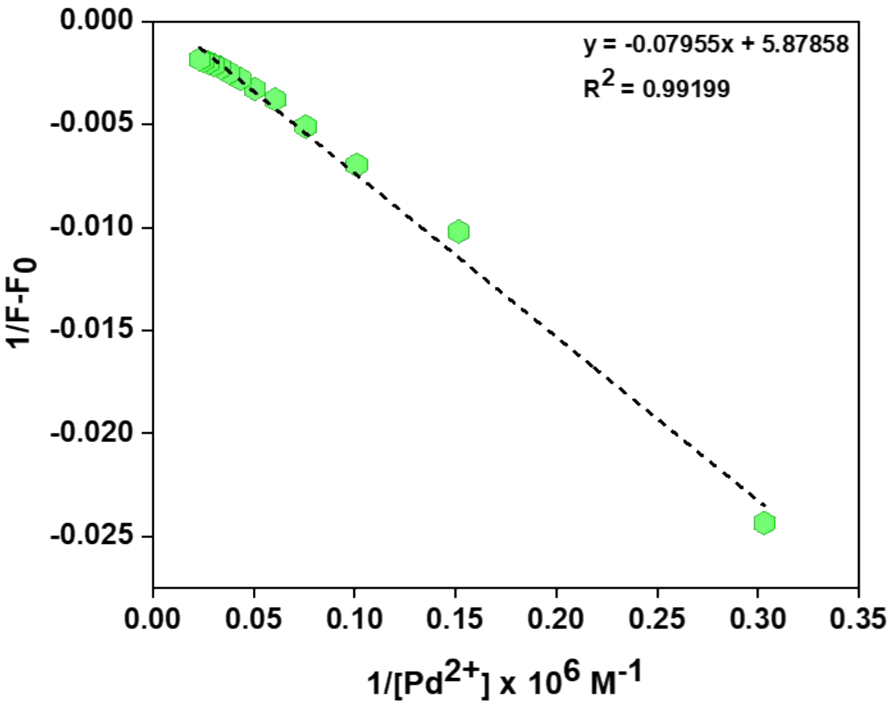

Fig. S24. Benesi-Hildebrand plot for determination of binding constant of **AnQn**-Pd^{2+}.

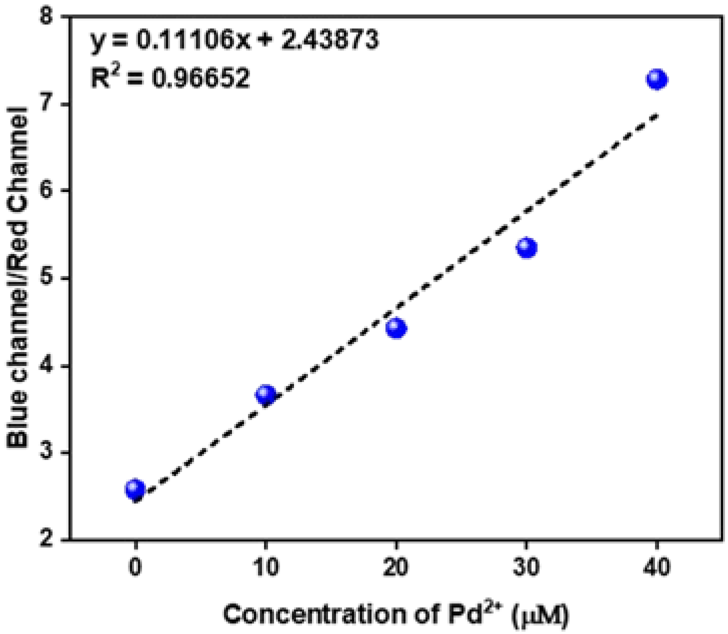

Fig. S25. Plot of RGB values (Blue/Red channel) and concentration of Pd^{2+} for determination of detection limit in solid state.

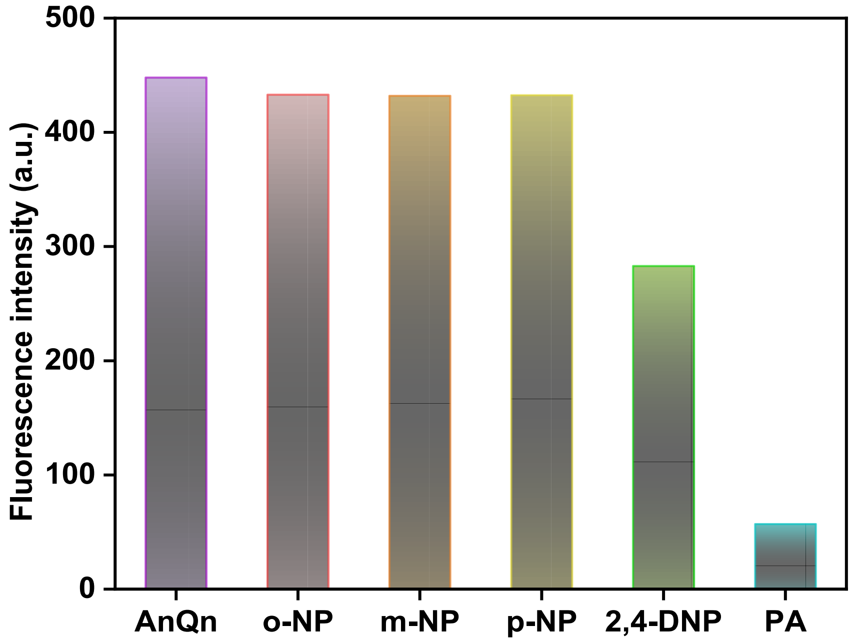

Fig. S26. Bar diagram showing changes in PL intensity of **AnQn** in presence of different nitroaromatic compounds (*o*-NP: *ortho*-nitrophenol; *m*-NP: *meta*-nitrophenol; *p*-NP: *para*-nitrophenol; 2,4-DNP: 2,4-dinitrophenol and PA: picric acid).

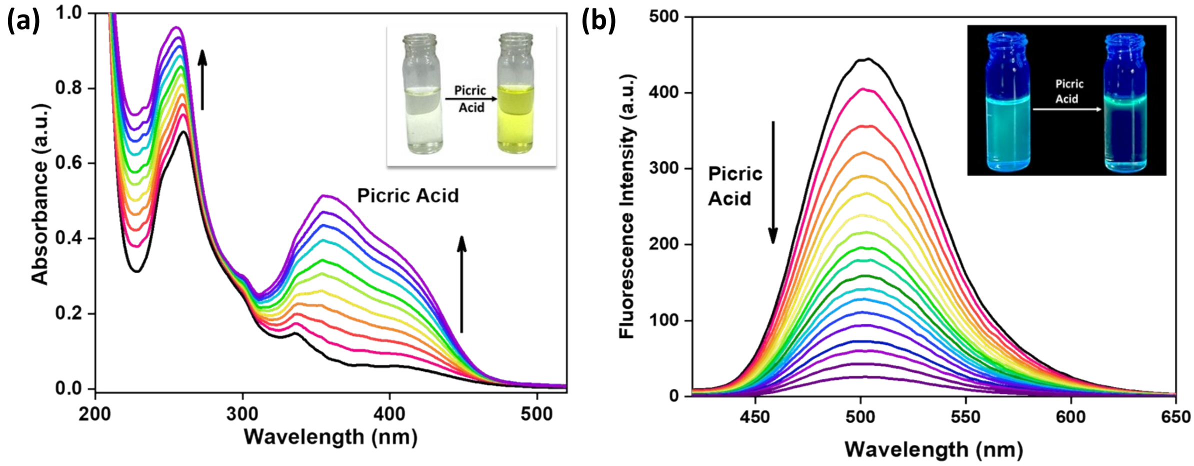

Fig. S27. (a) Absorption and (b) fluorescence titration curves of **AnQn** with picric acid (PA).

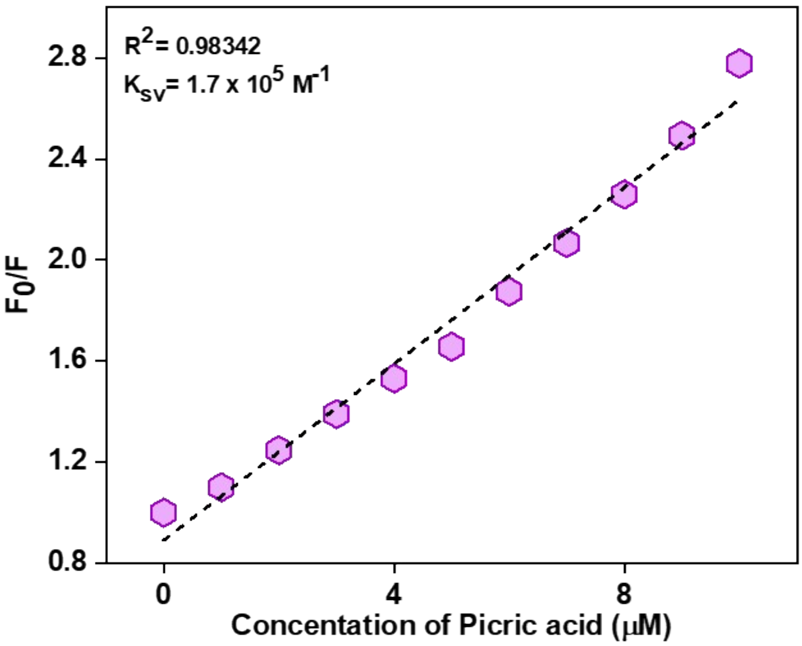

Fig. S28. Stern-Volmer plot for quenching of **AnQn** upon successive addition of picric acid.

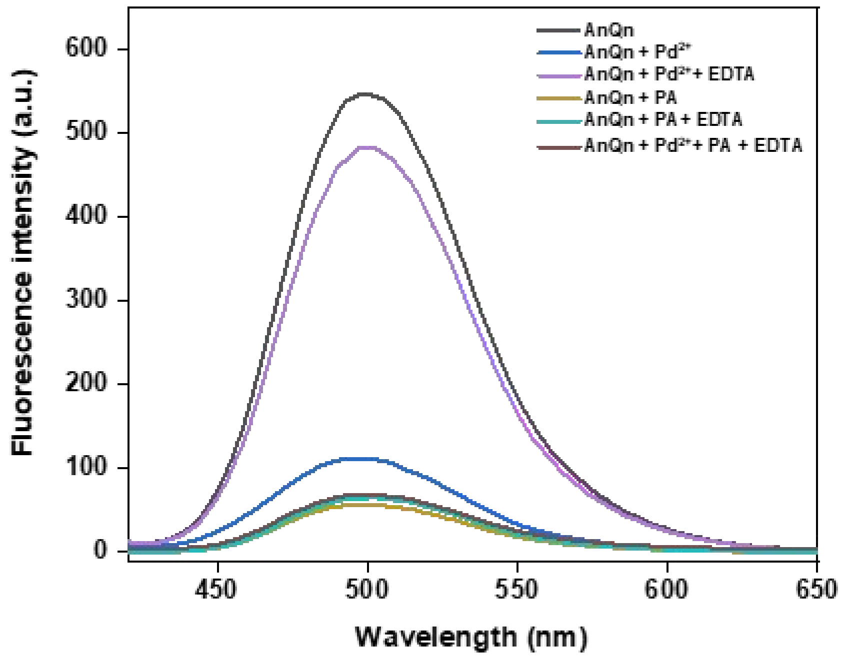

Fig. S29. Discriminative fluorescence sensing of PA over Pd^{2+} ions using EDTA as a masking agent.

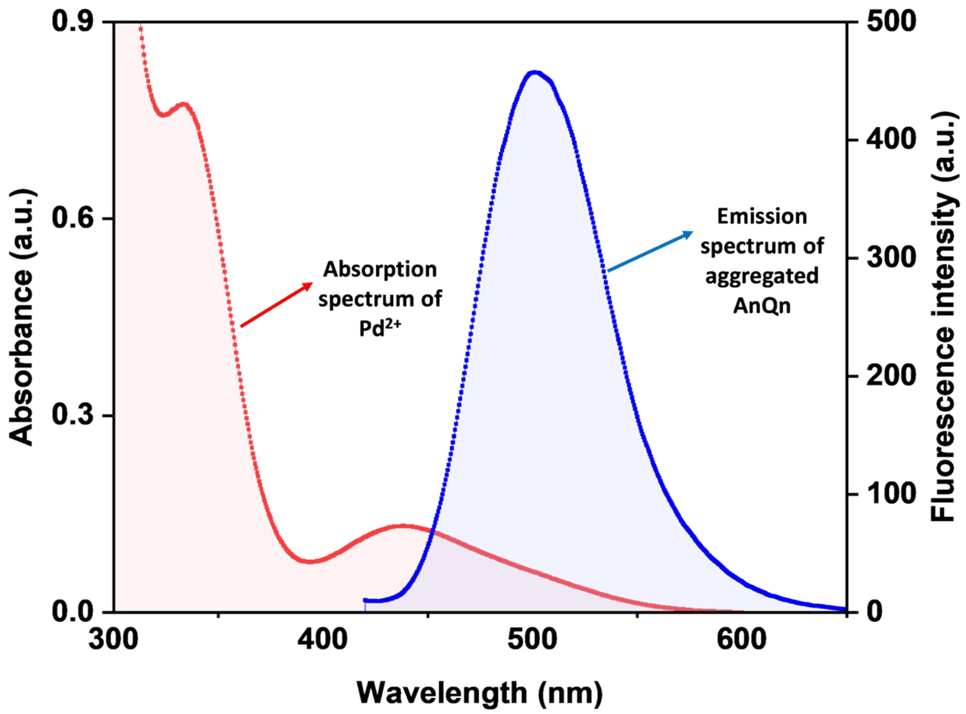

Fig. S30. Absorption and emission spectra of Na_2PdCl_4 and **AnQn** aggregates.

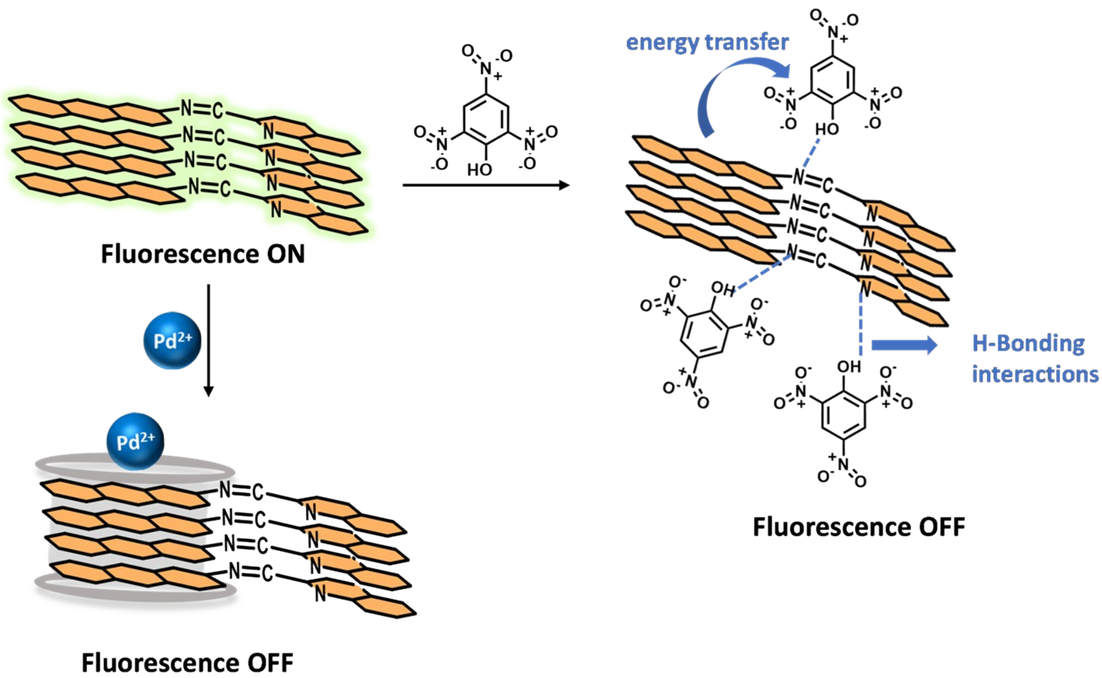

Fig. S31. Plausible mechanistic pathway for fluorescence quenching of aggregated **AnQn** with Pd^{2+} and picric acid.

Table S7. Determination of Pd^{2+} in different samples of water using emission study.

Real Sample	Pd^{2+} added (µM)	Pd^{2+} detected (µM)	% Recovery
Tap water	8.33	8.26	99.15
	16.66	17.05	102.3
	25	24.39	97.56
River Water (S1)	8.33	7.05	84.63
	16.66	17.04	102.28
	25	22.6	90.4
River Water (S2)	8.33	8.32	99.8
	16.66	17.1	102.64
	25	22.19	88.7
Soil Water	8.33	8.2	98.7
	16.66	16.95	101.74
	25	23.9	95.6

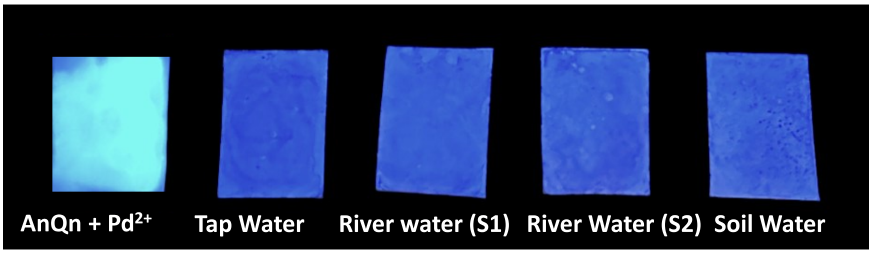

Fig. S32. Fluorescence detection of Pd^{2+} in different water samples on paper strips.

Table S8. Comparison of sensing parameters of probe **AnQn** with some previously reported probes.

Probe	Target ion	LoD (nM)	Binding constant	Application	Ref.
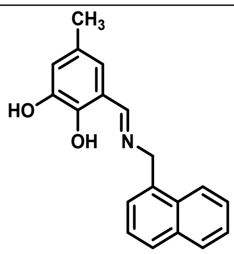	Al^{3+} Ga^{3+}	5860 5960	1.44×10^3 M^{-1} 1.25×10^2 M^{-2}	Paper strips Polystyrene Films	[1]
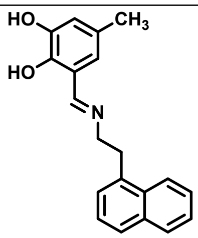	Al^{3+} Ga^{3+}	4640 3400	7.68×10^3 M^{-1} 1.27×10^2 M^{-2}	Paper strips Polystyrene Films	[1]
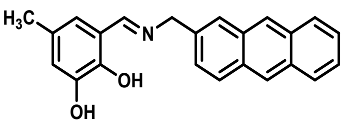	Al^{3+} Ga^{3+}	1460 1250	6.66×10^3 M^{-1} 1.43 x 10^3 M^{-2}	Paper strips Polystyrene Films	[1]
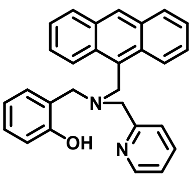	Al^{3+} Ga^{3+}	2.4 2.4	1.4×10^5 M^{-1} 1.0×10^5 M^{-1}	-	[2]

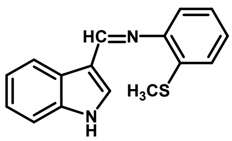	Al^{3+} Ga^{3+}	12.5 1600	1.81×10^{6} M^{-1} 1.64×10^{4} M^{-1}	Logic gate Paper strip Cell imaging	[3]
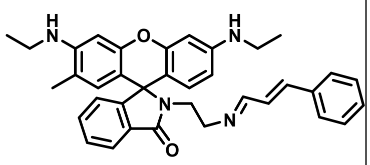	Al^{3+} Ga^{3+}	28 29	-	Paper strip Real sample analysis	[4]
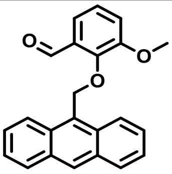 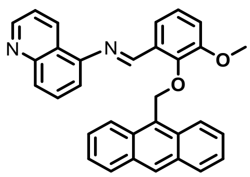	Al^{3+} Ga^{3+} Ga^{3+}	190 220 1310	3.58×10^{4} M^{-1} 2.80×10^{4} M^{-1} 2.24×10^{3} M^{-1}	Paper strips	[5]
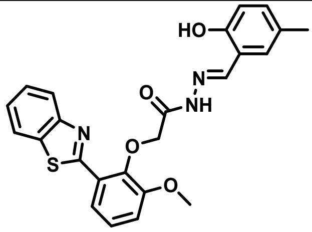	Al^{3+} Ga^{3+}	4510 8260	3.95×10^{4} M^{-1} 1.09 x 10^{4} M^{-1}	Paper strips Smartphone Cell imaging	[6]
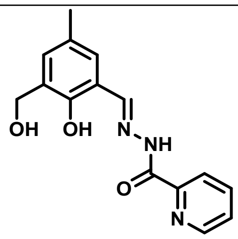	Al^{3+} Ga^{3+}	61.2 201	1.00×10^{9} M^{-1} 2.70×10^{11} M^{-1}	Logic gate Paper strips Cell imaging	[7]

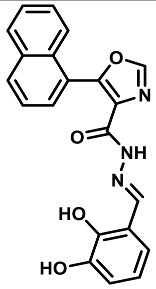	Al^{3+} Ga^{3+}	48.6 20	1.21×10^{10} M^{-2} 9.78×10^{8} M^{-2}	Real samples	[8]
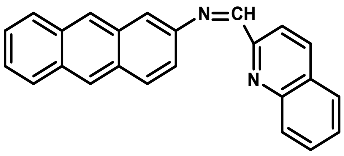	Al^{3+} Ga^{3+}	9.2 230	6.46×10^{5} M^{-1} 1.09×10^{5} M^{-1}	Logic gates Paper strips Real sample analysis	**Present study**

References:

[1] V. Kumar, P. Kumar, S. Kumar, D. Singhal, R. Gupta, Inorg. Chem. 58 (2019) 10364–10376.

[2] H. Kim, K.B. Kim, E.J. Song, I.H. Hwang, J.Y. Noh, P.G. Kim, K.D. Jeong, C. Kim, Inorg. Chem. Commun. 36 (2013) 72–76.

[3] Heena, V. Yadav, S. Saini, P. Roy, S. Layek, T. Goswami, S. Kumar, Chempluschem 89 (2024) e202300721.

[4] S. Ghosh, P. Roy, Anal. Methods 15 (2022) 17–26.

[5] H. Goyal, V. Kumar, A.K. Saini, G. Kedawat, B.K. Gupta, R. Gupta, Mater. Today Chem. 27 (2023) 101306.

[6] Q. Liu, Y. Liu, Z. Xing, Y. Huang, L. Ling, X. Mo, Spectrochim. Acta - Part A Mol. Biomol. Spectrosc. 287 (2023) 122076.

[7] S. Mishra, P. Mamidi, S. Chattopadhyay, A.K. Singh, J. Photochem. Photobiol. A Chem. 434 (2023) 114225.

[8] X. Guo, H. Han, Y. Xing, G. Zhang, J. Mol. Liq. 388 (2023) 122719.